Available online at www.sciencedirect.com
ScienceDirect
Nuclear Instruments and Methods in Physics Research B 252 (2006) 124–130
NIM B
Beam Interactions with Materials & Atoms
www.elsevier.com/locate/nimb

Cherenkov effect and parametric X-rays

A. Kubankin, V. Likhachev, N. Nasonov *, A. Rakitjansky, P. Zhukova

Laboratory of Radiation Physics, Belgorod State University, 14 Studencheskaya, 308007 Belgorod, Russia

Received 12 January 2006; received in revised form 27 June 2006
Available online 28 August 2006

Abstract

Self-diffracted Cherenkov X-rays emitted from relativistic electrons penetrating into the periodic multilayer nanostructure are considered in this work. A distinction is made between this radiation and known parametric X-rays for Bragg scattering geometry.

PACS: 41.50.Th; 78.70.−g

Keywords: Cherenkov radiation; Parametric X-rays; Periodic nanostructure

1. Introduction

Coherent scattering of the Coulomb field associated with a fast charged particle moving through a medium with periodically changing dielectric susceptibility $\chi(\omega,\mathbf{r}) = \chi_0(\omega) + \sum_g' \chi_g(\omega) e^{i\mathbf{g}\cdot\mathbf{r}}$ brings into existence the electromagnetic radiation known as the parametric X-rays (PXR) [1–3]. Traditionally, PXR is considered as a source of quasimonochromatic X-rays in the frequency range where $\chi_0(\omega) < 0$. The emission process in this event is characterized by the strong difference between dispersion laws for primary virtual photon of emitting particle Coulomb field and for real photons of emission field. It is therefore concluded that the condition of Bragg resonance between primary and secondary photons cannot be asserted exactly (resulting in suppression of the manifestation of dynamical diffraction effects in PXR). The situation can be changed substantially in the vicinity of a photoabsorption edge of target's material where the average dielectric susceptibility $\chi_0(\omega)$ can take positive values and the Cherenkov effect becomes possible. In conditions of Cherenkov effect the nature of primary and secondary photons in PXR process is the same. Because of this the role of dynamical diffraction effects in PXR increases. Particularly, an essential growth of PXR yield can be realized in conditions under discussion [4] due to the modification of the effect of anomalous photoabsorption in PXR.

The result [4] has been obtained for Laue scattering geometry. Meanwhile, the Bragg scattering geometry is more adequate for real experiment. Indeed, the inequality $\chi_0(\omega) > 0$ for X-rays can be fulfilled above all in the range of soft X-rays ($\omega \sim 100$ eV), therefore the period of used periodical structures must exceed substantially the value common to the distance between atoms in a crystal. The most suitable of such structure are one-dimensional multilayer nanostructures used in X-ray optics. Obviously, only the Bragg scattering geometry can be realized in an experiment devoted to PXR generation from the multilayer nanostructure. The task being discussed is considered in this work.

The main goal of our studies is to show the strong modification of PXR spectral–angular distribution in the vicinity of a photoabsorption edge of target's material where the real part of the medium dielectric susceptibility can take positive values. Distinctions between the diffraction of virtual and Cherenkov photons are analyzed in detail. In addition to this the possibility to generate an intense X-ray beam on the base of proposed approach is shown.

* Corresponding author. Tel.: +7 4722 315726; fax: +7 4722 311213.
E-mail address: nnn@bsu.edu.ru (N. Nasonov).

0168-583X/$ - see front matter
doi:10.1016/j.nimb.2006.06.034

The paper is organized as follows. In Section 2 we present the general expression for the total emission amplitude including the contribution of parametric and diffracted transition radiation mechanisms. The general analysis of the peculiarities in emission characteristics caused by anomalous dispersion of target's dielectric susceptibility is performed in Section 3. The results of numerical calculations are presented in Section 4. Our conclusions are given in Section 5.

2. General expressions

Let us consider an emission from relativistic electrons penetrating into the target as it is shown in Fig. 1. In the case of a one-dimensional structure consisting of alternative layers with thicknesses a and b and susceptibilities χ_a and χ_b respectively, the quantities $\chi_0(\omega)$ and $\chi_{\mathbf{g}}(\omega)$ determining the periodically changing dielectric susceptibility of the multilayer nanostructure are given by the expressions

$$\begin{aligned}\chi_0(\omega) &= \frac{a}{T}\chi_a + \frac{b}{T}\chi_b, \quad \chi_{a,b} = \chi'_{a,b} + \mathrm{i}\chi''_{a,b},\\ \chi_{\mathbf{g}}(\omega) &= \frac{1-\mathrm{e}^{\mathrm{i}\mathbf{g}\cdot\mathbf{a}}}{\mathrm{i}gT}(\chi_a - \chi_b),\end{aligned} \tag{1}$$

where $T = a + b$ is the period of multilayer structure, $\mathbf{g} = \mathbf{e}_x g$, $g = (2\pi/T)n$, $n = 0, \pm 1, \pm 2, \ldots, \mathbf{e}_x$ is the normal to the surface of the target (see Fig. 1).

To determine the emission properties one should find the Fourier-transform of the electric field

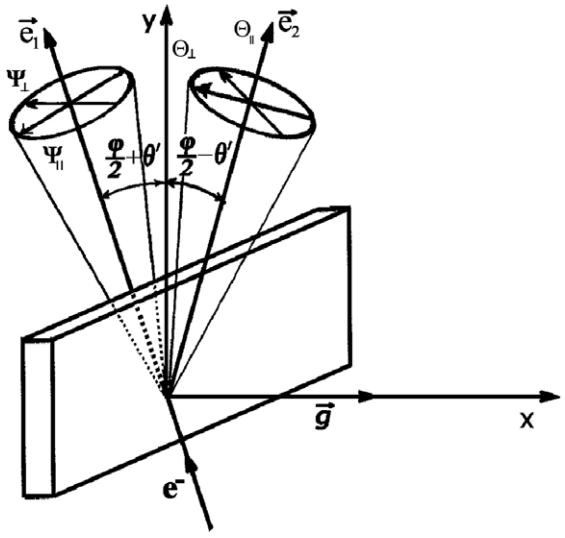

Fig. 1. The geometry of the emission process. A multilayer nanostructure is positioned at the Bragg condition in an electron beam, $\mathbf{g}$ is the reciprocal lattice vector, $\mathbf{e}_1$ is the electron-beam axis, $\mathbf{e}_2$ is the photon collimator axis, φ is the emission angle, θ' is the orientation angle, which may be changed by the goniometer, $\Theta_\parallel$ and $\Psi_\parallel$ are the components of the angular variables $\mathbf{\Theta}$ and $\mathbf{\Psi}$ parallel to the plane, determined by the vectors $\mathbf{e}_1$ and $\mathbf{e}_2$, $\Theta_\perp$ and $\Psi_\perp$ are the components perpendicular to such a plane.

$$\mathbf{E}_{\omega\mathbf{k}} = (2\pi)^{-4}\int \mathrm{d}^3 r\,\mathrm{d}t\,\mathrm{e}^{\mathrm{i}\omega t - \mathrm{i}\mathbf{k}\cdot\mathbf{r}}\mathbf{E}(\mathbf{r},t), \tag{2}$$

by means of the ordinary Maxwell equation

$$\begin{aligned}&(k^2 - \omega^2(1+\chi_0))\mathbf{E}_{\omega\mathbf{k}} - \mathbf{k}(\mathbf{k}\cdot\mathbf{E}_{\omega\mathbf{k}}) - \omega^2\sum_{\mathbf{g}}{}' \chi_{-\mathbf{g}}\mathbf{E}_{\omega\mathbf{k}+\mathbf{g}}\\ &\quad = \frac{\mathrm{i}\omega e}{2\pi^2}\mathbf{V}\delta(\omega - \mathbf{k}\cdot\mathbf{V}),\end{aligned} \tag{3}$$

where $\mathbf{V}$ is the emitting electron velocity. Within the framework of two-wave approximation of dynamical diffraction theory the system (3) is reduced to simple equations

$$\begin{aligned}&(k^2 - \omega^2(1+\chi_0))E_{\lambda 0} - \omega^2\chi_{-g}\alpha_\lambda E_{\lambda g}\\ &\quad = \frac{\mathrm{i}\omega e}{2\pi^2}\mathbf{e}_{\lambda 0}\cdot\mathbf{V}\delta(\omega - \mathbf{k}\cdot\mathbf{V}),\\ &((\mathbf{k}+\mathbf{g})^2 - \omega^2(1+\chi_0))E_{\lambda g} - \omega^2\chi_g\alpha_\lambda E_{\lambda 0} = 0,\end{aligned} \tag{4}$$

where new quantities have been defined by the expressions

$$\begin{aligned}&\mathbf{E}_{\omega\mathbf{k}} = \sum_{\lambda=1,2}\mathbf{e}_{\lambda 0}E_{\lambda 0}, \quad \mathbf{E}_{\omega\mathbf{k}+\mathbf{g}} = \sum_{\lambda=1,2}\mathbf{e}_{\lambda g}E_{\lambda g},\\ &\mathbf{e}_{10} = \mathbf{e}_{1g} = \frac{\mathbf{k}_\parallel\times\mathbf{e}_x}{k_\parallel}, \quad \mathbf{e}_{20} = \frac{\mathbf{k}\times\mathbf{e}_{10}}{k}, \quad \mathbf{e}_{2g} = \frac{(\mathbf{k}+\mathbf{g})\times\mathbf{e}_{10}}{|\mathbf{k}+\mathbf{g}|},\\ &\alpha_1 = 1, \quad \alpha_2 = \frac{\mathbf{k}\cdot(\mathbf{k}+\mathbf{g})}{k|\mathbf{k}+\mathbf{g}|}, \quad \mathbf{k} = \mathbf{e}_x k_x + \mathbf{k}_\parallel, \quad \mathbf{e}_x\mathbf{k}_\parallel = 0,\end{aligned} \tag{5}$$

Eq. (4) describes the electromagnetic field inside the multilayer structure. The corresponding wave equations for field components $E^{\mathrm{V}}_{\lambda 0}$ and $E^{\mathrm{V}}_{\lambda g}$ in the vacuum outside the target follow from (4) in the limit $\chi_0 = \chi_{\mathrm{g}} = 0$.

The solution of the task being considered has been obtained, for example, in [5] for semi-infinite absorbing crystalline target and in [6] for the multilayer nanostructure with a finite thickness. In the case of high-absorbing target under consideration the model of semi-infinite multilayer nanostructure is quite adequate, so we are entitled to use the results [5,6]. Following [5] one can obtain the final expression for the Fourier-transform of diffracted field in the vacuum $E^{\mathrm{V}}_{\lambda g}$ in the form

$$\begin{aligned}&E^{\mathrm{V}}_{\lambda g} = a_{\lambda\mathbf{k}_\parallel}\delta\left(k_x + g - \sqrt{\omega^2 - k_\parallel^2}\right),\\ &a_{\lambda\mathbf{k}_\parallel} = \frac{\mathrm{i}\omega^3 e\chi_g\alpha_\lambda}{4\pi^2 p^2|V_x|}\frac{\mathbf{e}_{\lambda 0}\cdot\mathbf{V}}{\Delta \pm \kappa_\lambda - \frac{\omega^2}{p}\chi_0}\left[\frac{1}{\frac{1}{V_x^2}(\omega - \mathbf{k}_\parallel\cdot\mathbf{V}_\parallel + pV_x) + \frac{1}{2}(\Delta \mp \kappa_\lambda)}\right.\\ &\qquad\left. - \frac{1}{\frac{1}{V_x^2}(\omega - \mathbf{k}_\parallel\cdot\mathbf{V}_\parallel + pV_x)}\right],\\ &\kappa_\lambda = \sqrt{\left(\Delta - \frac{\omega^2}{p}\chi_0\right)^2 - \frac{\omega^4}{p^2}\chi_g\chi_{-g}\alpha_\lambda^2},\\ &p = \sqrt{\omega^2 - k_\parallel^2}, \ \Delta = g\left(\frac{g}{2p} - 1\right).\end{aligned} \tag{6}$$

The sign ($\pm$) in (6) depends on the solution of dynamical diffraction task and will be determined below. To find the emission amplitude $A_{\lambda\mathbf{n}}$ one should calculate

Fourier-integral $E_\lambda^{\mathrm{Rad}} = \int \mathrm{d}^3 k_g \mathrm{e}^{\mathrm{i}\mathbf{k}_g\mathbf{n}r} E_{\lambda g}^{\mathrm{V}}|_{r\to\infty} \to A_{\lambda\mathbf{n}} \frac{\mathrm{e}^{\mathrm{i}\omega r}}{r}$ ($\mathbf{k}_g = \mathbf{k} + \mathbf{g}$, $\mathbf{n}$ is the unit vector to the direction of emitted photon propagation). Calculating Fourier-integral by the stationary phase method and using the angular variables φ, θ', $\boldsymbol{\Theta}$ and $\boldsymbol{\Psi}$ presented in Fig. 1 one can obtain the final formula for the emission amplitude

$$A_\lambda = \frac{e}{\pi} \frac{\chi_g \alpha_\lambda \Omega_\lambda}{\tau \pm \delta_\lambda - \mathrm{i}\chi_0''} \left(\frac{1}{\gamma^{-2} + \Omega^2} - \frac{1}{\gamma^{-2} - \chi_0' + \Omega^2 - \tau \mp \delta_\lambda} \right), \tag{7}$$

where γ is the Lorentz factor of the emitting electron, $\tau = 2\sin^2\left(\frac{\varphi}{2}\right)\left(\frac{\omega_{\mathrm{B}}'}{\omega} - 1\right) - \chi_0'$, $\omega_{\mathrm{B}}' = \omega_{\mathrm{B}}\left(1 + (\theta' + \Theta_\parallel) ctg\left(\frac{\varphi}{2}\right)\right)$, $\omega_{\mathrm{B}} = \frac{g}{2\sin\left(\frac{\varphi}{2}\right)}$ is the Bragg frequency, $\Omega^2 = \Omega_1^2 + \Omega_2^2$, $\Omega_1 = \Theta_\perp - \Psi_\perp$, $\Omega_2 = 2\theta' + \Theta_\parallel + \Psi_\parallel$, $\alpha_1 = 1$, $\alpha_2 = \cos\varphi$. The important quantity δ_λ proportional to κ_λ in (6) is determined by the formula

$$\delta_\lambda = \sqrt{\tau^2 - \beta_\lambda^2 - 2\mathrm{i}\chi_0''(\tau + \beta_\lambda \sigma_\lambda)}, \tag{8}$$

where $\beta_\lambda = \left(\sin\left(\pi\frac{a}{T}\right)/\pi\right)|\chi_a' - \chi_b'|\alpha_\lambda$, $\sigma_\lambda = \mathrm{sign}(\chi_a' - \chi_b') \times \left(\sin\left(\pi\frac{a}{T}\right)/\pi\right)(\chi_a'' - \chi_b'')\alpha_\lambda/\chi_0''$. Returning to the general formula for the emission amplitude A_λ it should be noted that the top sign in front of the coefficient δ_λ corresponds to the frequency range where $\tau(\omega) > \beta_\lambda$ and the bottom sign corresponds to the inequality $\tau(\omega) < \beta_\lambda$.

Since formulae (7) and (8) constitute the basis for our further analysis, it would be well to elucidate the physical meaning of the parameters involved. It is easy to see that the quantity $\tau(\omega) + \chi_0'$ is proportional to so-called Bragg resonance defect Δ determined in (6) and describing the role of dynamical diffraction effects in PXR (these effects lead to the addition to wave vector of emitted photon proportional to $\tau \pm \delta_\lambda$). The coefficient β_λ is equal to $|\chi_g|\alpha_\lambda$. This coefficient determines the width of the region of anomalous dispersion $-\beta_\lambda < \tau < \beta_\lambda$ where the contribution of diffracted transition radiation is concentrated. The last coefficient σ_λ is well known in the dynamical diffraction theory. It describes the effect of anomalous photoabsorption.

3. PXR and self-diffracted Cherenkov radiation

Two emission mechanisms contribute to total emission amplitude A_λ, determined by (7). There are diffracted transition radiation and PXR. Since Cherenkov radiation of interest to us is realized outside the frequency range $-\beta_\lambda < \tau(\omega) < \beta_\lambda$ we can consider PXR contribution separated from that of diffracted transition radiation. Let us represent the total amplitude A_λ as a sum of two components

$$\begin{aligned} A_\lambda &= A_\lambda^{\mathrm{DTR}} + A_\lambda^{\mathrm{PXR}}, \\ A_\lambda^{\mathrm{DTR}} &= \frac{e}{\pi} \frac{\chi_g \alpha_\lambda}{\tau \pm \delta_\lambda - \mathrm{i}\chi_0''} \Omega_\lambda \left(\frac{1}{\gamma^{-2} + \Omega^2} - \frac{1}{\gamma^{-2} - \chi_0 + \Omega^2} \right), \\ A_\lambda^{\mathrm{PXR}} &= -\frac{e}{\pi} \frac{\chi_g \alpha_\lambda}{\gamma^{-2} - \chi_0' + \Omega^2 - \tau \mp \delta_\lambda} \frac{\Omega_\lambda}{\gamma^{-2} - \chi_0 + \Omega^2}. \end{aligned} \tag{9}$$

The content of presented components of the total emission amplitude A_λ is clear. DTR amplitude is the product of the ordinary transition radiation field generated by a fast particle on a single boundary between a vacuum and the target with average dielectric susceptibility χ_0 into the reflection coefficient $\chi_g\alpha_\lambda/(\tau \mp \delta_\lambda - \mathrm{i}\chi_0'')$. PXR amplitude is the product of the equilibrium electromagnetic field associated with this particle moving through the target with average susceptibility (this field is the Coulomb field in the case $\gamma^{-2} - \chi_0' + \Omega^2 > 0$, or the Cherenkov radiation field if $\gamma^{-2} - \chi_0' + \Omega^2 < 0$) into the reflection coefficient $\chi_g\alpha_\lambda/(\gamma^{-2} - \chi_0' + \Omega^2 - \tau \mp \delta_\lambda)$ which testifies that PXR is generated into the volume of the target.

PXR spectral–angular distribution follows from (9) in the form

$$\omega \frac{\mathrm{d}^3 N_\lambda^{\mathrm{PXR}}}{\mathrm{d}\omega\, \mathrm{d}^2\Theta} = \frac{e^2}{\pi^2} \frac{\Omega_\lambda^2}{\left(\gamma^{-2} - \chi_0' + \Omega^2\right)^2 + \left(\chi_0''\right)^2} \times \frac{|\chi_g|^2 \alpha_\lambda^2}{\left(\gamma^{-2} - \chi_0' + \Omega^2 - \tau \mp \delta_\lambda'\right)^2 + \left(\delta_\lambda''\right)^2}. \tag{10}$$

At the beginning of our studies let us analyze the yield Eq. (10) in the case of ordinary PXR when $\chi_0' < 0$. In the case $\chi_0'' \ll |\chi_0'|$ under consideration result (10) can be reduced to more familiar form

$$\omega \frac{\mathrm{d}^3 N_\lambda^{\mathrm{PXR}}}{\mathrm{d}\omega\, \mathrm{d}^2\Theta} = \frac{e^2}{\pi} \frac{|\chi_g|^2 \alpha_\lambda^2}{\delta_\lambda''} \frac{\Omega_\lambda^2}{\left(\gamma^{-2} - \chi_0' + \Omega^2\right)^2} \times \delta(\gamma^{-2} - \chi_0' + \Omega^2 - \tau \mp \delta_\lambda'). \tag{11}$$

Well known approximation $(x^2 + \alpha^2)^{-1}|_{\alpha \ll 1} \to (\pi/\alpha)\delta(x)$ has been used when deriving (11). Here δ_λ' and δ_λ'' are real and imaginary parts of the function δ_λ defined in (8).

Performed analysis has shown that only the branch of possible solutions of PXR dispersion equation $\gamma^{-2} - \chi_0' + \Omega^2 - \tau \mp \delta_\lambda' = 0$ corresponding to top sign in front of the coefficient δ_λ' in this equation contributes to PXR yield in conditions $\chi_0' < 0$ under consideration. Moreover, this solution can be realized with the proviso that

$$\xi = \gamma^{-2} - \chi_0' + \Omega^2 > \beta_\lambda, \tag{12}$$

and has the form $\tau = \tau_* \approx ((\xi^2 + \beta_\lambda^2)/2\xi) > \beta_\lambda$. Taking into account the above inequality $\chi_0'' \ll |\chi_0'|$ one can obtain from (11) the final expression for PXR spectral–angular distribution

$$\omega \frac{\mathrm{d}^3 N_\lambda^{\mathrm{PXR}}}{\mathrm{d}\omega\, \mathrm{d}^2\Theta} = \frac{e^2\omega^2|\chi_g|^2}{4\pi \sin^2\frac{\varphi}{2}} \frac{1}{\omega\chi_0''} \frac{\Omega_\lambda^2 \alpha_\lambda^2}{\left(\xi + \beta_\lambda\sigma_\lambda\right)^2 + \beta_\lambda^2(1 - \sigma_\lambda^2)} \times \left(\frac{\xi^2 - \beta_\lambda^2}{\xi^2}\right)^2 \delta(\omega - \omega_{\mathrm{B}}'), \tag{13}$$

where the photon energy ω in δ-function is determined with an accuracy of γ^{-1} (in deriving on Eq. (13) it was assumed that $\chi_0' \sim \gamma^{-2}$).

Coefficient β_λ in (13) describes an influence of dynamical diffraction effects in PXR. It is easy to verify that result (13) coincides in the limit $\gamma^2\beta_\lambda \ll 1$ with well known kinematical

formula for PXR spectral–angular distribution [7]; otherwise the role of such effects can be essential. Among other things, an influence of the effect of anomalous photoabsorption increases in the case $\sigma_\lambda \approx 1$ [8].

It is significant to keep in mind that the inequality (12) is a necessary condition for X-ray generation on the branch corresponding to top sign in (11) independently on the sign of χ'_0, specifically, PXR on the branch being considered can be excited in the range of anomalous dispersion of target's material where $\chi'_0 > 0$. It should be noted in this connection that only PXR in high frequency range where $\chi'_0 \approx -\omega_0^2/\omega^2 < 0$ (ω_0 is the average plasma frequency of the target) was studied up to now. This approach is adequate for PXR from a crystal because the Bragg frequency ω_B in the vicinity of which PXR spectrum is concentrated has a typical value $\omega_B \sim 10$ keV in the case in question. On the other hand, the macroscopical multilayer nanostructure being studied in this work as a radiator for X-ray producing allows to generate X-rays in low frequency range of the order of tens or hundreds electron volt. Photoabsorption edges of many elements are brought into this frequency range in the vicinity of which the susceptibility χ' can take positive values.

In this paper we would like to call attention to some peculiarities in PXR existing under conditions discussed. The effect of PXR suppression in the range of small observation angles primarily follows from (12) and (13). Indeed, the condition $\xi > \beta_\lambda$ (12) can be rewritten as $\Omega^2 > \chi'_0 + \beta_\lambda - \gamma^{-2}$. Since $|\chi'_0| > \beta_\lambda$, the quantity $\chi'_0 + \beta_\lambda - \gamma^{-2}$ is negative in the case $\chi'_0 < 0$ independently on the energy of emitting electron, so that Ω^2 can take arbitrary values. On the other hand, in the case $\chi'_0 > 0$ the region of acceptable values of Ω^2 is bounded underside for high enough energies of emitting electrons $\gamma > 1/\sqrt{\chi'_0 + \beta_\lambda}$.

To illustrate the predicted effect let us consider PXR angular distribution versus the sign of the average dielectric susceptibility χ'_0. For simplicity sake assume that $\Psi_\perp = \Psi_\parallel = \Theta_\parallel = \theta' = 0$, $\varphi = \pi/2$, so that only σ-polarization makes a contribution to PXR yield, $(a/T) \ll 1$ and $\chi_a \sim \chi_b$, so that $\beta_1 \approx \frac{a}{T}|\chi'_a - \chi'_b| \ll |\chi'_0| \approx |\chi'_b|$ and $\sigma_1 \ll 1$. In addition to this the energy of emitting electron is assumed to be high enough, so that $\gamma^2|\chi'_0| \gg 1$. In accordance with (13) PXR angular distribution is described in conditions under consideration by the functions $F^{(\pm)}(x,y)$

$$\frac{\mathrm{d}^2 N^{\mathrm{PXR}}}{\mathrm{d}^2\Theta} = \frac{e^2\omega|\chi'_0|}{4\pi\sin^2(\varphi/2)}\frac{1}{\omega\chi''_0}F^{\pm}(x,y),$$
$$F^{\pm}(x,y) = \frac{y^2x^2}{(x^2\pm 1)^2 + y^2}\frac{\left[(x^2\pm 1)^2 - y^2\right]^2}{(x^2\pm 1)^4}, \tag{14}$$

where $x = \Theta_\perp/\sqrt{|\chi'_0|}$, $y = a|\chi'_a - \chi'_b|/T|\chi'_0|$, the function $F^{(+)}$ should be used if $\chi'_0 < 0$; otherwise one should use the function $F^{(-)}$. The curves 1 and 2 presented in Figs. 2 and 3 demonstrate the shift of PXR angular distribution in the case $\chi'_0 > 0$ to the side of large observation angles and the growth of local emission density as compared with that in the case $\chi_0 < 0$.

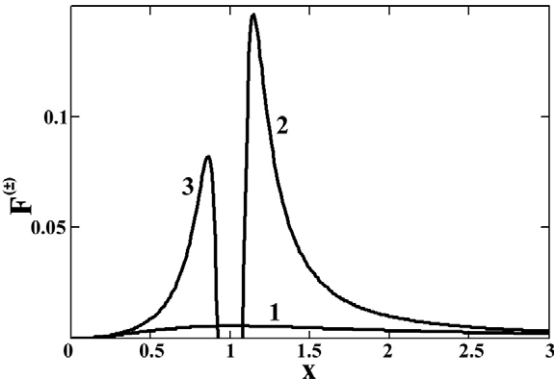

Fig. 2. Influence of the dispersion of dielectric susceptibility on PXR angular distribution. The presented curves were calculated for $y = 0.15$. Curve 1 describes the ordinary PXR for $\chi'_0 < 0$; Curve 2 corresponds to the PXR but for $\chi'_0 > 0$; Curve 3 describes DCR.

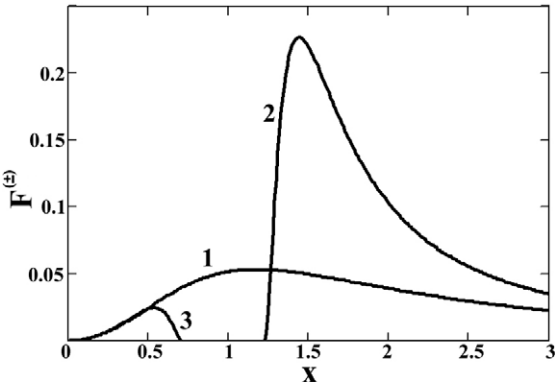

Fig. 3. Influence of the dispersion of dielectric susceptibility on PXR angular distribution. The presented curves were calculated for $y = 0.5$. Curve 1 describes the ordinary PXR for $\chi'_0 < 0$; Curve 2 corresponds to the PXR but for $\chi'_0 > 0$; Curve 3 describes DCR.

Turning back to the general formula (11) let us consider the emission properties under conditions $\xi < 0$, when the emitting electron climbs over Cherenkov threshold. Performed analysis has shown that the emission excited in the case in question connects with the additional branch of PXR dispersion equation corresponding to bottom sign in front of the coefficient δ'_λ in the argument of δ-function in (11). A necessary condition for X-ray generation analogous to (12) has the form

$$\xi = \gamma^{-2} - \chi'_0 + \Omega^2 < -\beta_\lambda. \tag{15}$$

As this takes place the solution of the dispersion equation $\tau = \tau_* = (\xi^2 + \beta_\lambda^2)/2\xi$ arrives at the range $\tau < -\beta_\lambda$ different from that for the ordinary PXR. In contrast with (12) the condition (15) constrains possible values of observation angles from overhead. This property is an essential advantage of the emission mechanism covered as compared to ordinary PXR, since it allows to produce X-ray beams with higher average angular density.

To show the main dissimilarities of such self-diffracted Cherenkov radiation (DCR) from the ordinary PXR let us consider the emission angular distribution. DCR

spectral–angular distribution follows from (11) in the form (13) in accordance with performed analysis, but for different range of ω and Ω designated by the condition (15) instead of (12). Integrating the distribution derived over ω and using the same assumptions as for PXR above one can obtain the following formula:

$$\frac{d^2N^{DCR}}{d^2\Theta} = \frac{e^2\omega\chi_0'}{4\pi\sin^2\left(\frac{\varphi}{2}\right)}\frac{1}{\omega\chi_0''}F^{(-)}(x,y), \tag{16}$$

where the function $F^{(-)}(x,y)$ is defined in (14), but in contrast with $F^{(-)}(x,y)$ from (14) where the argument x is varied through a range $x > \sqrt{1+y}$, the field of variation of $F^{(-)}(x,y)$ from (15) is determined by inequalities $0 < x < \sqrt{1-y}$.

The curves presented in Figs. 2 and 3 allow one to elucidate an influence of the dispersion of target's dielectric susceptibility on PXR properties. Curve 1 in these figures illustrates the angular distribution of ordinary PXR realizing in the frequency range where $\chi_0'(\omega) < 0$, that is PXR far from the vicinity of a photoabsorption edge. Curve 2 corresponds to PXR in the vicinity of a photoabsorption edge where the average dielectric susceptibility of the target $\chi_0'(\omega)$ is positive but the condition of Cherenkov effect is not fulfilled. As noted above, the maximum of PXR angular distribution is shifted to the side of large observation angles in going from the frequency range far from the vicinity of a photoabsorption range to this vicinity where the strong dispersion of the dielectric susceptibility $\chi_0(\omega)$. In addition to this, the growth in PXR intensity is realized due to the dispersion of $\chi(\omega)$, what is more important for the problem of effective X-ray source creation on the base of PXR emission mechanism. In keeping with presented figures the relative enhancement of PXR yield due to the dispersion effect is particularly high under conditions of small values of the parameter y.

Curve 3 in the figures describes DCR angular distribution. The main advantage of DCR as compared with PXR consists in more narrow angular distribution of emitted photon flux. The curves presented in Fig. 2 show that DCR yield can exceed substantially that of ordinary PXR for small values of the parameter y, but the total DCR yield is always less than that of PXR modified by dispersion effect occurring near to Cherenkov threshold. As may be seen from Fig. 3, the relative contribution of DCR becomes negligible in the range of large enough values of the parameter y.

Performed analysis allows to describe the general properties of PXR process under conditions of anomalous dispersion of target's dielectric susceptibility $\chi(\omega)$. It is of interest to estimate the possibility to observe predicted peculiarities in PXR process in a real experiment. The corresponding results of numerical calculations performed on the base of the general formula for emission amplitude (7) and frequency-dependence of real and imaginary parts of the dielectric susceptibility $\chi(\omega)$ determined by an experimental approach are presented in the next section of this paper.

4. The results of numerical calculations

One of the main questions in the task being discussed consists of the correct choosing of the material for the periodic nanostructure. Such choose depends strongly in the needed energy of emitted photons. As a result of our searches the periodical nanostructure consisting of alternating layers of Si and Ca was found to be suitable for DCR and PXR generation in the frequency range $\omega \approx 100$ eV by electrons of intermediate energy of the order of 10 MeV. The frequency-dependence of dielectric susceptibilities $\chi_{Ca}(\omega)$ and $\chi_{Si}(\omega)$ are presented in Fig. 4 [9]. The presented curves show the possibility to realize DCR and PXR processes in the vicinity of Si photoabsorption L-edge. The period of nanostructure was chosen in such a way that the Bragg frequency was close to 100 eV. The ratio a/T (Ca was chosen as a material of the lager with the thickness a) was equal to 0.1 in our calculations. Obviously, in the case being considered the average dielectric susceptibility χ_0' can take positive and negative values versus the frequency ω.

It is important to keep in mind that PXR, DCR and diffracted transition radiation are liable to contribute simultaneously to the formation of total emission yield. Therefore we have used in the performed calculations the general formula for the emission spectral–angular distribution:

$$\begin{aligned}\omega\frac{d^3N_\lambda}{d\omega d^2\Theta} &= \frac{e^2}{\pi^2}\frac{|\chi_g|^2\Omega_\lambda^2\alpha_\lambda^2}{\left(\tau+\mathrm{sign}(\tau-\beta_\lambda)\delta_\lambda'\right)^2+\left(\chi_0''-\mathrm{sign}(\tau-\beta_\lambda)\delta_\lambda''\right)^2}\\ &\times\left[\frac{1}{\left(\gamma^{-2}+\Omega^2\right)^2}-\frac{1}{\left(\gamma^{-2}-\chi_0'+\Omega^2-\tau-\mathrm{sign}(\tau-\beta_\lambda)\delta_\lambda'\right)^2+\left(\delta_\lambda''\right)^2}\right.\\ &\left.\times\left(1-2\frac{\chi_0'+\tau+\mathrm{sign}(\tau-\beta_\lambda)\delta_\lambda'}{\gamma^{-2}+\Omega^2}\right)\right],\end{aligned} \tag{17}$$

following from (7). Formula (17) was used for calculations of the emission properties under conditions when the nanostructure was arranged in exact Bragg position relative to incident electron beam ($\theta' = 0$, see Fig. 1) and the emission angle φ was equal to $\pi/2$ (only σ-polarization contributes to the emission yield in the case being considered). Although formula (17) allows to describe an influence of

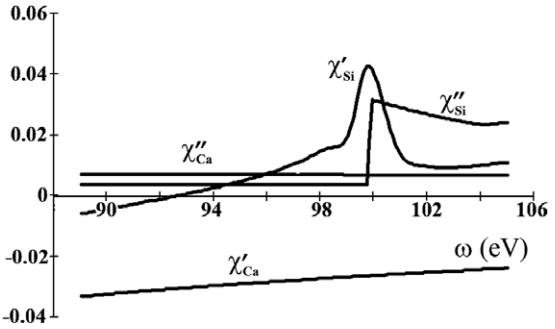

Fig. 4. The frequency-dependence of the real and imaginary parts of average dielectric susceptibilities of Ca and Si.

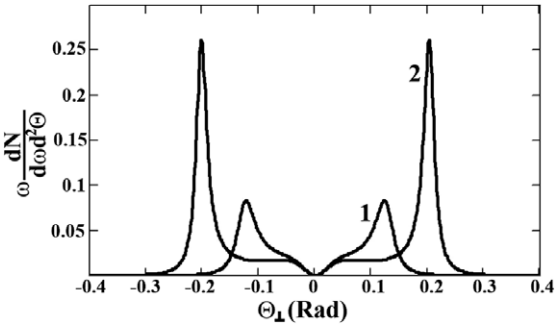

Fig. 5. DCR (curve 1) and PXR (curve 2) angular distributions for fixed energy of emitted photon in condition $\chi_0' > 0$. The presented curves were calculated for fixed parameters $\omega = 99.5$ eV, $a/T = 0.1$, $\gamma = 20$, $\Theta_{\parallel} = \theta' = 0$, $\varphi = \pi/2$ and different Bragg frequency $1 - \omega_B = 101.9$ eV, $2 - \omega_B = 103.3$ eV.

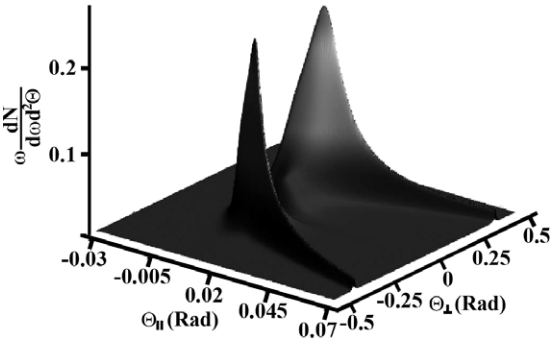

Fig. 6. Two-dimensional angular distribution of DCR for fixed parameters $\omega = 99.5$ eV, $a/T = 0.1$, $\gamma = 20$, $\omega_B = 101.9$ eV, $\theta' = 0$, $\varphi = \pi/2$.

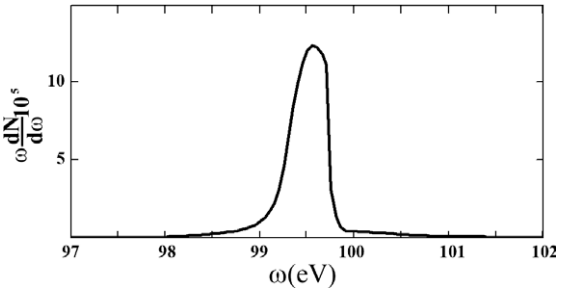

Fig. 7. The spectrum of collimated DCR. The presented curve was calculated for fixed parameters $\Delta\Theta_{\perp} = 0.1$ rad, $\Delta\Theta_{\parallel} = 0.02$ rad, $\gamma = 20$, $a/T = 0.1$, $\varphi = \pi/2$, $\omega_B = 101.9$ eV, $\theta' = 0$. The angular position of collimator's axis corresponds to the optimal case $\Theta_{\parallel}^{axis} = 0.01$ rad, $\Theta_{\perp}^{axis} = 0.2$ rad.

multiple scattering of emitting electrons, this influence was ignored in the performed calculations as a negligibly small effect.

Angular distributions of the total emission calculated by the general formula (17) for several fixed values of the photon energy ω are presented in Fig. 5. Curve 1 corresponds to DCR contribution with account of the additional contribution of diffracted transition radiation which is small in the frequency range considered outside the range of anomalous dispersion. Curve 2 describes PXR modified by dispersion effects. As may be seen from Fig. 5, PXR intensity exceeds substantially that of DCR. This conclusion coincides with that outlined above (see Figs. 2 and 3). On the other hand, angular size of emitted DCR photon flux is significantly less than that of PXR.

It should be noted that the dispersion of dielectric susceptibility $\chi_0'(\omega)$ influences essentially on the manifestation of dynamical diffraction effects in PXR. As mentioned above, such effects are described by the coefficient β_λ in (7) and subsequent formulae (it is easy to verify that the general formula (13) is reduced in the limit $\beta_\lambda \to 0$ to well known kinematic formula for PXR spectral–angular distribution [7]). The role of the effects being discussed is not very high in the frequency range where $\chi_0'(\omega) < 0$. Indeed, the function $F^{(+)}(x,y)$ from Eq. (14) is approximately equal to kinematic function $y^2x^2/(x^2+1)^2$ for small values of the parameter $y \sim \beta_1$ (see curve 1 in Figs. 2 and 3). On the other hand, there are dramatic changes in PXR spectral–angular distribution caused by dynamical diffraction effects in the vicinity of a photoabsorption edge where the susceptibility $\chi_0'(\omega)$ can be positive. Such changes described by the function $F^{(-)}(x,y)$ for both PXR and DCR branches are illustrated by curves 2 and 3 in Figs. 2 and 3. Moreover, dynamical changes increase with decreasing of the parameter y, as indicated by the comparison of the curves presented in Figs. 2 and 3.

Above discussed dynamical effects can involve a specific form of PXR two-dimensional angular distribution. This distribution calculated by the general formula (17) for DCR branch is illustrated in Fig. 6.

Let us consider PXR spectrum in the vicinity of a photoabsorption edge that is of prime concern to applications. The spectrum of collimated PXR is presented in Fig. 7. A point that should be mentioned is the high spectral–angular density of PXR under conditions of strong dispersion of dielectric susceptibility. Indeed, the total number of quanta, emitted in conditions under considerations ($N \approx 10^{-6}$ ph./el., this yield is typical for PXR) is concentrated in angular cone $\Delta\Theta = 2 \times 10^{-3}$ sterad. On the other hand, the angular size of ordinary PXR from electrons with the same energy is about $(2\gamma^{-1})^2 = 4 \times 10^{-2}$ sterad. In such a manner, the spectral–angular density of PXR realizing in the vicinity of a photoabsorption edge can exceed essentially that of ordinary PXR.

5. Conclusion

In accordance with performed analysis, PXR properties can be modified very substantially in the frequency range, where the real part of average dielectric susceptibility of the target $\chi_0'(\omega)$ takes positive values.

Only one from two possible branches of the solution of PXR dispersion equation can contribute to the formation of PXR yield under conditions when an emitting electron does not overcome the Cherenkov threshold. Nevertheless, the emission properties are very different versus the sign of $\chi_0'(\omega)$.

An influence of dynamical diffraction effects increases substantially in the case $\chi'_0(\omega) > 0$ (more exactly $\chi'_0(\omega) > \gamma^{-2}$). As this takes place, PXR spectral–angular density is suppressed in the range of small observation angles, but the local density can increase significantly in the range of large angles. The condition $\Theta^2 - \beta_\lambda > \chi'_0(\omega) - \gamma^{-2} > 0$ seems to be most appropriate for PXR producing.

The emission excited under conditions when the emitting electron climbs over Cherenkov threshold corresponds to the additional branch of PXR dispersion equation banned for ordinary PXR. The main distinctive feature of the emission being discussed consists in its narrow angular distribution as compared with ordinary PXR or PXR in the vicinity of a photoabsorption edge but before Cherenkov threshold.

The total yield of such DCR emission is comparable with that of the ordinary PXR.

Acknowledgements

This work was accomplished in the context of both the program "Advancement of the scientific potential of high education" by Russian Ministry of Education and Science (Project RNP.2.1.1.3263) and fund RFBR (Grants: 06-02-16714 and 06-02-16942). One of the authors (A.K.) is grateful to the Belgorod State University for the Internal grant (VKG 026-06). The authors are very grateful to the referee for useful criticism.

References

[1] M.L. Ter-Mikaelian, High Energy Electromagnetic Processes in Condensed Media, Wiley, New York, 1972.
[2] G.M. Garibian, C. Yang, Sov. Phys. JEPT 34 (1972) 495.
[3] V.G. Baryshevsky, I.D. Feranchuk, Sov. Phys. JEPT 34 (1972) 502.
[4] N. Nasonov, P. Zhukova, Phys. Lett. A 346 (2005) 367.
[5] A. Caticha, Phys. Rev. B 45 (1992) 9541.
[6] N. Nasonov, V. Kaplin, S. Uglov, M. Piestrup, C. Gary, Phys. Rev. E 68 (2003) 03654.
[7] I. Feranchuk, A. Ivashin, J. Phys. (Paris) 46 (1985) 1981.
[8] N. Nasonov, Phys. Lett. A 292 (2001) 146.
[9] B.L. Henke, E.M. Gullikson, J.C. Davis, At. Data Nucl. Data Tables 54 (1993).